

1, 2 AND 3 DIMENSIONAL PHOTONIC MATERIALS MADE USING ION BEAMS: FABRICATION AND OPTICAL DENSITY-OF-STATES

M.J.A. DE DOOD¹, L.H. SLOOFF¹, T.M. HENSEN¹, D.L.J. VOSSEN¹,
A. MOROZ^{1,3}, T. ZIJLSTRA², E.W.J.M. VAN DER DRIFT², A. VAN
BLAADEREN^{1,3} AND A. POLMAN¹

¹ *FOM Institute for Atomic and Molecular Physics
Kruislaan 407
1098 SJ Amsterdam, The Netherlands*

² *Delft Institute for Microelectronics and Submicron Technology
P.O. Box 5053
2600 GB Delft, The Netherlands*

³ *Debye Institute, Utrecht University
Padualaan 8
3584 CH Utrecht, The Netherlands*

1. Introduction

The spontaneous emission rate of an optical probe atom is strongly dependent on its optical environment. This concept is well known in one-dimensional geometries, e.g. for an atom placed near a mirror, a dielectric interface, or in a microcavity.¹⁻⁶ With the recent development of two- and three-dimensional photonic crystals it becomes possible to tailor optical modes and the local optical density-of-states (DOS) to a much greater extent. Large effects on the spontaneous emission rate of optical probe ions are expected in these materials.

In order to study these effects, accurate and reproducible methods of optical doping must be developed. Ion implantation is a technique with which ions can be introduced at a well-defined depth and concentration into any material, in a reproducible fashion. In this paper we demonstrate this concept for Cr ions implanted near the surface of an Al₂O₃ single crystal. In this one-dimensional system the DOS near the interface can be calculated from Fermi's Golden rule. It can be experimentally varied by bringing liquids with different refractive index in contact with the crystal surface, as we will show. In this way it becomes possible to determine the radiative decay rate and quantum efficiency of Cr in Al₂O₃. These well-characterized samples can then be used to study the changes in spontaneous emission in more complicated systems such as absorbing and strongly scattering materials. We also study the DOS in a one-dimensional system with two interfaces: a SiO₂ thin film on a Si substrate. Er ions are implanted in the SiO₂ thin film, and their radiative decay rate is derived from experiments in which the DOS is varied. Using these data it becomes possible to study the effect of a varying DOS in a 3-dimensional system composed of Er-doped SiO₂ colloidal particles. Large effects on the spontaneous emission rate are observed, as will be shown. Finally, we will discuss the design and fabrication of two-dimensional photonic crystals in silicon. A method to incorporate a luminescent dye in these crystals is described which may be used to study the DOS.

2. Spontaneous Emission near a Dielectric Interface

Experimental

Single crystal (0001) oriented α -Al₂O₃ substrates were implanted with 150 keV Cr⁺ ions at room temperature to fluences of 0.6, 1.6, 2.5, 3.0 and 4.0×10¹⁵ at/cm². The samples were rotated by 7° with respect to the ion beam to avoid ion channeling along the [0001] crystal direction. After implantation, the samples were annealed at 1450 °C for 2 hours in air. PL measurements were performed using the 457.9 nm line of an Ar ion laser as an excitation source and by collecting the PL signal using a 48 cm monochromator with a spectral resolution of 3.3 cm⁻¹ in combination with a GaAs photomultiplier tube. The Ar ion laser was modulated at 13 Hz using an acousto-optic-modulator. Luminescence decay traces were recorded using the photomultiplier tube in combination with a multichannel photon counting system. The overall time resolution was 400 ns.

SiO₂ layers, of 100 nm thickness, were grown on Si(100) substrates in two consecutive steps, using a solution of 10.5 ml ethanol, 0.3 ml water (29 wt.% NH₃), and 0.4 ml TEOS under continuous stirring. The layers were then implanted with 70 keV Er ions to a fluence of 3.4×10¹⁴ at/cm², resulting in a Gaussian depth profile with a peak concentration of 0.22 at.% peaking at a depth of 39 nm and a standard deviation of 11 nm. The implanted layers were annealed at 100 °C for 1h and 900 °C for 1h in a vacuum furnace.

Silica colloids with a diameter of 339 nm and a polydispersity of 5% were synthesized under similar reaction conditions as described by van Blaaderen.⁷ After synthesis the colloidal particles were kept in pure ethanol. A layer of these colloidal particles was deposited on a Si substrate by drying a droplet of this suspension on the substrate. This resulted in a layer consisting of 3-4 layers of stacked spheres as determined by Rutherford backscattering spectrometry (RBS) and scanning electron microscopy (SEM) measurements. The colloids were implanted with 350 keV Er to a fluence of 1.5×10¹⁵ at/cm². The projected ion range of the 350 keV Er is 200 nm. After implantation the samples were annealed at 100 °C for 1h and 900 °C for 1h in a vacuum furnace to optically activate the Er ions.⁸ Photoluminescence (PL) measurements were done by exciting the Er ions using the 488 nm line of an Ar ion laser. The PL signal was collected using a 48 cm monochromator in combination with a liquid nitrogen cooled Ge detector, using standard lock-in techniques at a modulation frequency of 13 Hz. PL decay traces were recorded and averaged at the peak of the Er luminescence at 1.536 μm using a digitizing oscilloscope. The overall time resolution was 30 μs.

Various liquid films with different refractive index, ranging from n = 1.33 to n = 1.57, were brought in contact with the implanted side of both the Er implanted and Cr implanted samples. A ~1 mm thick liquid film was created by holding a liquid droplet between the sample and a fused silica slide. The luminescence signal was collected from the back. Using the same setup, the SiO₂ colloids were index matched by using a glycerol-water-mixture with a refractive index of 1.45, and photoluminescence decay traces were measured.

Results and Discussion

Characteristic luminescence, around $\lambda = 694$ nm, from Cr³⁺ doped Al₂O₃ occurs if the Cr ions are incorporated as substitutional atoms on the Al sublattice in the Al₂O₃ crystal lattice. Because the electrons involved in the transition are the outer lying 3d electrons, the transition wavelength is extremely sensitive to the local electronic environment provided by the surrounding atoms. After annealing the Cr implanted samples show the characteristic R line luminescence at wavelengths of 694.3 and 692.9 nm. It was found that the luminescence intensity of ion implanted samples increased with increasing fraction of substitutional Cr ions, as measured by RBS channeling measurements.⁹

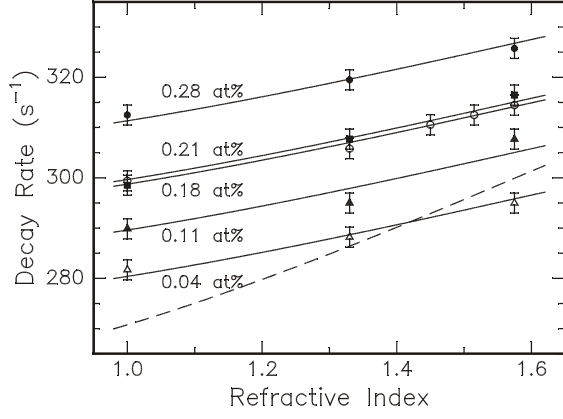


Figure 1: Measured decay rate for Cr implanted Al_2O_3 samples brought in contact with liquids with different refractive indices. The dashed line shows the calculated variation of the decay rate assuming only radiative decay at a rate of 310 s^{-1} . The solid line is a fit through all data points assuming a constant radiative decay rate but a different non-radiative decay rate for each Cr concentration, resulting in a radiative decay rate of $164 \pm 10 \text{ s}^{-1}$.

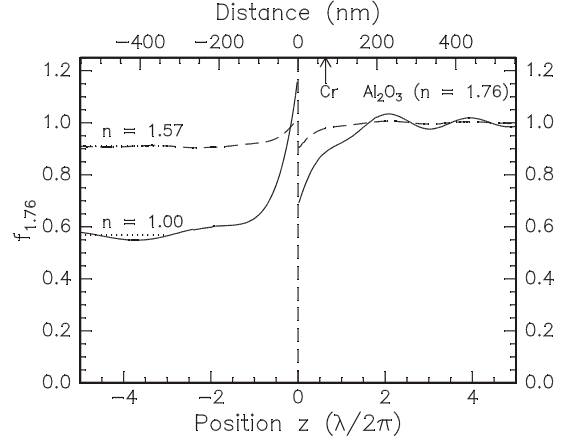


Figure 2: Polarization- and angle-averaged optical DOS $f_{1.76}$ as function of position, calculated for an Al_2O_3 sample brought in contact with air ($n = 1.00$) and a liquid with a refractive index of 1.57. The optical DOS was normalized to the optical DOS in bulk Al_2O_3 ($n = 1.76$). The arrow indicates the peak of the Cr distribution.

The decay rate of the R_1 line luminescence at 694.3 nm was measured for samples brought in contact with liquids with different refractive indices. The luminescence decay can be described as a single-exponential over at least 4 orders of magnitude within experimental error. Figure 1 shows the measured decay rate as a function of the refractive index of the liquid for samples with different Cr peak concentrations. All samples show a similar increase in the decay rate with refractive index of the liquid, independent of the Cr concentration. The total measured decay rate (W) is composed of the sum of radiative and non-radiative decay rates:

$$W = W_{rad} + W_{non-rad} . \quad (1)$$

The increase of the decay rate with refractive index can be explained by calculating the density of optical modes for ions close to the interface as function of the position z from the interface. Using the electric dipole approximation for the coupling between the atom and the electromagnetic field, the spontaneous emission rate can be given with the use of Fermi's Golden Rule,^{5,10,11}

$$W_{rad}(z) = \frac{\pi \omega}{\hbar \varepsilon(z)} |D|^2 \rho(\omega, z), \quad (2)$$

where D is the dipole matrix element of the atomic transition between the excited state and the ground state at a transition frequency ω . ρ is the polarization- and angle-averaged local density-of-states (DOS)¹² at position z from the interface and $\varepsilon(z)$ is the position dependent dielectric constant. The matrix element D is determined by the local electronic environment of the emitting ion and is not influenced by the optical properties of the interface. Note that the presence of the interface does not affect the local-field as studied in Ref. 13. Therefore, the only parameter varied in our experiment is the local DOS at a fixed frequency.

The changes in the radiative decay rate can be expressed using an optical DOS which differs by a factor ε from the local DOS defined above.¹⁴ Using this optical DOS, the total decay rate for an ion at position z can be written as:

$$W(n, z) = f_{1.76}(n, z)W_{rad}^{1.76} + W_{non-rad}, \quad (3)$$

where $f_{1.76}$ denotes the optical DOS, normalized to the optical DOS for bulk Al_2O_3 with a refractive index of 1.76. $W_{rad}^{1.76}$ is the radiative decay rate in bulk Al_2O_3 .

Figure 2 shows the calculated optical DOS as a function of the distance z from the interface. The solid line shows the calculation for an infinite half space of Al_2O_3 ($n = 1.76$) brought in contact with an infinite half-space of air ($n = 1.00$). The interface is positioned at $z = 0$. The dashed line shows a calculation for Al_2O_3 in contact with a medium with a refractive index of 1.57. The optical DOS is discontinuous at the interface due to the discontinuity in the contribution of the polarization component that is parallel to the interface¹¹. The oscillations observed on both sides are caused by interference between incoming and reflected waves and have a periodicity of $\sim \lambda/2n$. The peak position of the Cr distribution is indicated by the arrow. As can be seen, the radiative decay rate is suppressed towards the interface and increases for increasing refractive index at the position of the Cr ions.

The effect of the optical DOS on the radiative lifetime was obtained by integrating the optical DOS over depth using the known Cr depth distribution. This calculation was repeated for refractive indices of the liquid in the range 1.0-1.76. The result of this calculation is shown by the dashed line in Fig. 1, assuming a radiative decay rate of 310 s^{-1} for Cr ions in bulk Al_2O_3 and no non-radiative decay ($W_{non-rad} = 0$). The value of 310 s^{-1} was arbitrarily chosen such that the calculated variation of the radiative decay rate can be compared to the experimental data. As can be seen by comparing the dashed line with the data, the slope in the data cannot be described by assuming radiative decay only. The data can be fitted if non-radiative decay rate is introduced as given by Eq. (3). The solid lines show a single fit to all data, assuming the same radiative rate for all Cr concentrations, but a different non-radiative rate, resulting in a radiative decay rate $W_{rad}^{1.76} = 164 \pm 10 \text{ s}^{-1}$ for bulk Al_2O_3 . The corresponding non-radiative decay rate increases linearly from 137 to 168 s^{-1} with Cr concentration. These well characterized samples will be used to measure changes in spontaneous emission induced by absorbing or strongly scattering media where theory is less well developed.

Similar experiments were performed by bringing 100 nm thick SiO_2 layers implanted with erbium in contact with a range of transparent liquids. After annealing, the Er implanted samples show clear luminescence at a wavelength of $1.536 \mu\text{m}$, related to the transition from the $^4\text{I}_{13/2}$ first excited state to the $^4\text{I}_{15/2}$ ground state of the Er^{3+} ion. The measured decay rate for liquids with different refractive indices is shown in Fig. 3. The inset shows the experimental setup, where the Er ions are pumped from the front and the PL signal is collected from the back of the sample, through the silicon substrate. As for the Cr doped Al_2O_3 an increase of the decay rate with refractive index of the liquid is observed.

Calculations of the optical DOS for a thin film geometry involving two interfaces were done.¹¹ Because the refractive index of the SiO_2 layer ($n = 1.45$) is much lower than that of the Si substrate ($n = 3.44$), the structure does not support guided modes in the SiO_2 layer. It was found that for a 100 nm thick SiO_2 film on Si the optical DOS for a wavelength of $1.5 \mu\text{m}$ increases in the entire SiO_2 film, when the refractive index of the liquid is increased. No oscillations of the optical DOS in the SiO_2 film are observed because the film thickness is much smaller than the wavelength of emission. However, the optical DOS in the layer is significantly increased with respect to the bulk value due to the presence of the high index Si substrate.

The effect of the position-dependent optical DOS was integrated over the film thickness using the known Er depth distribution and the known distribution of the 488 nm pump laser light through the film. The non-radiative decay rate was assumed to be

independent of the refractive index of the covering liquid. The solid line in Fig. 3 shows a best fit to the data by assuming a radiative decay rate of 69 s^{-1} and a non-radiative decay rate of 115 s^{-1} . The difference between the solid line and the dashed line shows the calculated variation of the radiative decay rate as a function of the refractive index of the covering liquid. The radiative decay rate of the Er ions in the SiO_2 layer of $69 \pm 10 \text{ s}^{-1}$ can be converted into a radiative decay rate for Er ions in bulk SiO_2 of $48 \pm 10 \text{ s}^{-1}$ using the known optical DOS of the layer structure. This value is lower than that for the layer, because the high refractive index Si substrate increases the optical DOS in the SiO_2 film.

Using the now known radiative decay rate of Er ions in SiO_2 prepared via a wet chemical process, changes in the Er decay rate can now be used to probe the optical DOS in systems where theory to calculate the optical DOS is less well developed. Figure 4 shows luminescence decay traces measured at a wavelength of $1.536 \mu\text{m}$ for an Er-implanted colloidal particle (340 nm diameter) in air and in contact with an index matching liquid ($n = 1.45$). A clear increase in the decay rate from 69 s^{-1} to 101 s^{-1} is observed when the spheres are index matched. The inset shows a SEM image, taken from the top, that shows the arrangement of the colloidal spheres on the Si substrate. Some local ordering of the spheres in a hexagonal pattern is visible.

The difference in the measured decay rates is caused by a change in the optical DOS, assuming that the non-radiative decay rate is independent of the optical surrounding. The optical DOS can be calculated for the index matched spheres, where the problem reduces to the problem of a single interface between Si ($n = 3.44$) and SiO_2 ($n = 1.45$). The result of that calculation shows that the influence of the interface is negligible ($< 6\%$) at the position of the Er ions, so that the radiative decay rate is the same as that for bulk SiO_2 . In absence of non-radiative decay, it would be concluded that the index matching liquid increases the radiative decay rate by a factor of 1.5 (from 69 to 101 s^{-1}). However, using the radiative decay rate determined from the 100 nm thick SiO_2 film of $48 \pm 10 \text{ s}^{-1}$, we obtain a non-radiative decay rate of $53 \pm 10 \text{ s}^{-1}$. Using this non-radiative decay rate the radiative decay rate will be suppressed from $48 \pm 10 \text{ s}^{-1}$ ($101-53$), for the index matched sample, to $16 \pm 10 \text{ s}^{-1}$ ($69-53$) for the same sample in air. This corresponds to a factor 2-4 increase of the radiative decay rate due to the presence of the liquid. Note that the extremely low radiative decay rate of Er in silica is partly due to the fact that the colloids are surrounded by air ($n = 1.0$).

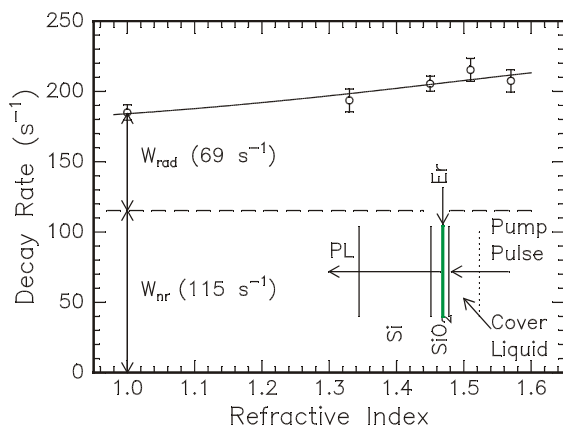


Figure 3: Measured decay rate of Er ions implanted into a 100 nm thick SiO_2 layer brought in contact with liquids with different refractive indices. The data can be fitted using the calculated optical DOS, resulting in a radiative decay rate of $69 \pm 10 \text{ s}^{-1}$ and a non-radiative decay rate of $115 \pm 10 \text{ s}^{-1}$. The inset shows the experimental setup.

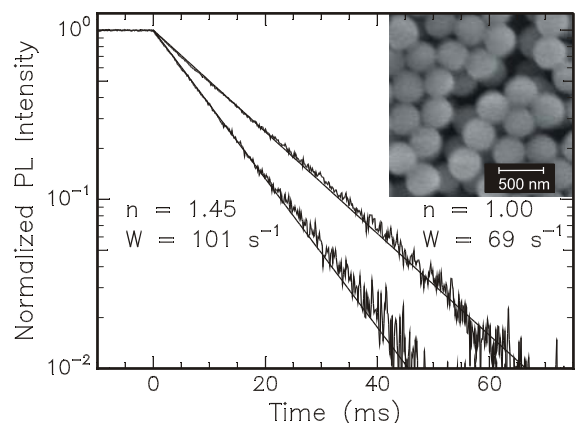


Figure 4: Luminescence decay traces for Er implanted SiO_2 colloidal spheres of 339 nm diameter. The inset shows a SEM image of the sample looking from the top. A clear increase in decay rate is observed when the spheres are index matched using a water-glycerol mixture with $n = 1.45$.

3. 2-D Photonic Crystals

Band Structure Calculations

Figure 5 shows the structure of a 2-D photonic crystal of infinitely long cylinders on a square lattice. Indicated in the figure are the cylinder radius r and pitch a . The photonic bandstructure of this structure was calculated using the transfer matrix method,¹⁵ for different dielectric constant ϵ of the rods and for various values of the radius-to-pitch ratio r/a . The bandstructure was calculated for transverse magnetic (TM) polarization (E field along the cylinder axis) and transverse electric (TE) polarization (E field perpendicular to the cylinder axis). The definition of TM and TE polarization is indicated in the right side of Fig. 5. For sufficiently high dielectric constant of the rods, such a structure shows photonic bandgaps for TM polarization only,¹⁶ i.e., no waves with TM polarization can propagate in any direction perpendicular to the rods. One interesting application of the square lattice of rods is the fabrication of a 90° waveguide bend.^{17,18}

Figure 6 shows the calculated bandstructure for a lattice of Si rods ($\epsilon = 11.8$, $n = 3.44$) for $r/a = 0.18$. A photonic bandgap is observed for TM polarization extending from $\omega a/2\pi c = 0.30$ to 0.44 . Bandstructure calculations repeated for different r/a and ϵ show that bandgaps for TM polarization exist for $\epsilon > 3.8$ ($n > 1.95$),¹⁹ which is just out of reach of standard polymers and glasses. Therefore, silicon seems a natural choice because of its high refractive index and because microfabrication technology is well developed for this material. The optical bandgap energy of Si is 1.1 eV, corresponding to a vacuum wavelength of $\sim 1.1 \mu\text{m}$, consequently Si is transparent in the near-infrared, which allows for fabrication of devices operating at the standard telecommunication windows at 1.3 and 1.5 μm .

For devices operating at a wavelength of 1.5 μm , a lattice constant of 570 nm is required, with a corresponding diameter of 205 nm of the rods. For proper vertical confinement in the photonic crystal index guiding may be used. This could be achieved using amorphous Si ($n = 3.74$) on Si ($n = 3.44$).¹⁹ Using dielectric waveguide theory to calculate the modes of such a waveguide, it is concluded that the rods need to be etched at least 5 μm deep through a 2 μm thick amorphous silicon layer to prevent light from leaking to the substrate.

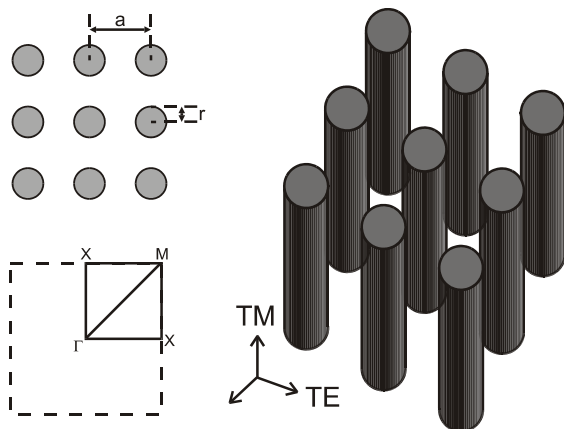


Figure 5: Square lattice of dielectric cylinders with radius r and pitch a . The Γ , X, and M points of symmetry in the square Brillouin zone are indicated in the left side of the figure. The electric field vector for transverse magnetic (TM) and transverse electric (TE) polarization are indicated in the right side of the figure.

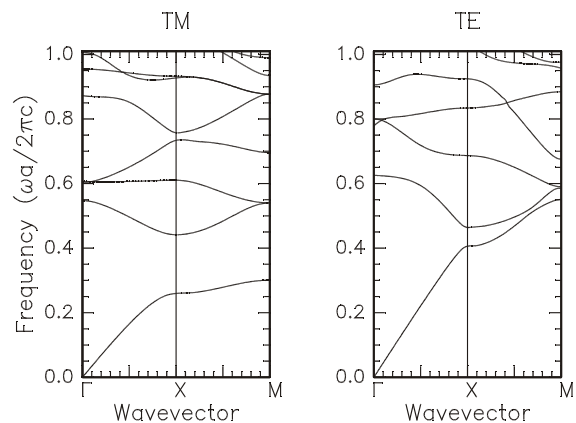


Figure 6: Calculated bandstructure along the ΓX and XM directions for a square lattice of Si cylinders ($n = 3.44$). A bandgap for TM polarization is observed from $\omega a/2\pi c = 0.30$ to 0.40 . No bandgaps are observed for TE polarization

Experimental

Amorphous Si (a-Si) layers on crystalline Si (c-Si) were obtained by irradiation of (100) oriented crystalline Si substrates with 4 MeV Xe ions at 77 K to a fluence of $2 \times 10^{15} \text{ cm}^{-2}$. Annealing at 500 °C for 1 hr in a vacuum furnace was performed to remove point defects and to relax the a-Si network structure,²⁰ to reach a thermally stable state with small absorption at 1.5 μm . The irradiation resulted in a 1.93 μm thick a-Si layer as measured by variable angle spectroscopic ellipsometry in the 300-1700 nm wavelength range. Rutherford backscattering spectrometry (RBS) measurements were done with a 2 MeV He^+ beam at a scattering angle of 165°.

All samples were coated with a resist double layer consisting of a 400 nm thick bottom layer of hardbaked AZ S1813 photoresist (Shipley) with an overlying 80 nm thick silicon containing negative tone e-beam resist SNR (Toyo Soda). Mask patterns were defined using e-beam lithography. After exposure (Leica EBPG05, 100 kV, $100 \mu\text{C cm}^{-2}$) the patterns were developed in xylene for 20 s followed by dipping in isopropyl-alcohol for 30 s to remove the unexposed areas. The pattern was then anisotropically transferred into the bottom resist layer by low pressure (0.3 Pa) oxygen reactive ion etching, using a plasma at a low rf power density of 0.07 W cm^{-2} (dc bias of -170 V). All patterning processes were controlled *in situ* by laser interferometry.

Anisotropic Si etching was accomplished in a SF_6/O_2 high density plasma using a distributed electron cyclotron resonance driven plasma setup (Alcatel DECR2000) operating at 2.45 GHz. He gas flowing at the back side of the substrate was used to control the temperature. The substrate was radio-frequency driven (13.56 MHz) for independent ion energy control towards the sample. Etching of the 2-D photonic crystal structures was achieved using a plasma of SF_6/O_2 (7.3:1.0) at 0.1 Pa, -97 °C substrate temperature, 400 W microwave power and -12 V dc bias, resulting in an etch rate of about 150 nm/min. At these conditions, mask selectivity is almost infinite. Scanning electron microscopy (SEM) images were taken with a 5.0 kV accelerating voltage, resulting in a resolution better than 5 nm.

In some cases the Si pillars were coated with a SiO_2 layer by immersing the photonic crystal sample in a solution of tetra-ethoxy-silane (TEOS, purity $\geq 99\%$), ammonia (29.1 wt.%), water, and ethanol. All substrates were cleaned using 2 M KOH in ethanol for 15 min and rinsed with pure ethanol prior to deposition. For incorporation of a fluorescent dye in the silica layer,^{7,21} 12.52 mg eosin-5-isothiocyanate (eosin-ITC) was first reacted with 41.8 mg (3-aminopropyl)-triethoxy-silane (APS) in 2.2 g dry ethanol by stirring for 16 h. Then 0.250 g of this mixture was added to a solution of 7.641 g ethanol, 0.809 g water, and 0.699 g ammonia. Next 0.380 g TEOS was added to the solution. All reactions took place at room temperature under continuous stirring. Fluorescence confocal microscopy (Leica TCS NT, 100 \times lens with NA 1.4) at excitation wavelengths of 476 and 488 nm was used to image the eosin-ITC coated silicon pillars.

Results and Discussion

Anisotropic etching of Si in a high density SF_6/O_2 plasma, using either an electron cyclotron resonance driven²² or inductively coupled plasma,²³ is a well understood process. The anisotropy is the result of involatile oxofluoride species. The overall etch profile is a delicate balance between etch product formation and ion-enhanced desorption. By changing the temperature, the oxygen flow and dc-bias separately at a given fluorine content, the dependence of the etching process on these parameters was optimized to great precision.²⁴

Figures 7a and b show SEM images of an array of 205 nm diameter silicon rods placed on a square lattice with a pitch of 570 nm, etched 5 μm deep. Figure 7a shows a square lattice in which a waveguide bend is defined by removing a row of rods from the square lattice. The row of rods removed to form a 90° waveguide bend is clearly visible. Such a

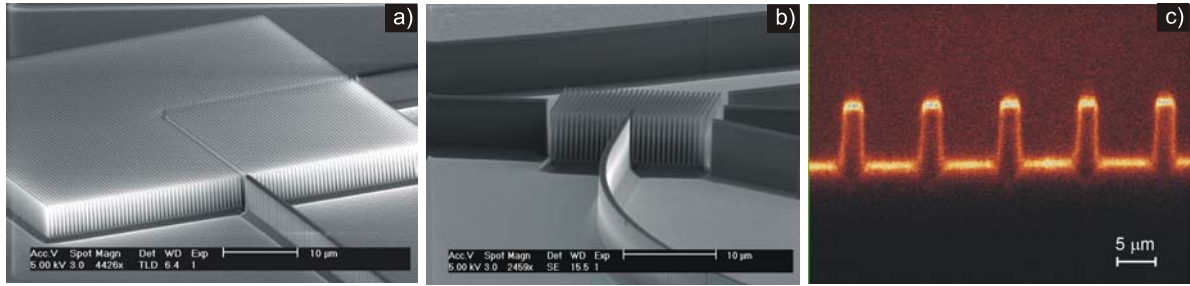


Figure 7: SEM images of a square lattice of Si cylinders of 205 nm diameter and a pitch of 570 nm, etched 5 μm deep (Figs. a) and b)). Figure a) shows a waveguide bend defined by removing a row of rods etched in crystalline Si, with input and output waveguide defined. Figure b) shows a similar bend structure etched through a 2 μm thick a-Si layer on c-Si. The waveguides serve to couple light in and out of the structure. Figure c) shows a cross-section made using confocal microscopy of a square lattice of micrometer size Si pillars, coated with a SiO_2 layer containing a luminescent dye (eosin-ITC).

line defect serves as a waveguide that can guide light around the corner with high efficiency¹⁷ with a bending radius that is much smaller than that of a conventional dielectric waveguide bend. Figure 7b shows an image of a similar device etched through an a-Si/c-Si stack. As can be seen the etching has proceeded continuous through the a-Si/c-Si interface, despite the fact that the etch rate of amorphous silicon is 30% lower than that of crystalline silicon. Waveguides to couple light in and out of the structure are integrated as well. They also include the 1.9 μm thick a-Si top layer that serves to confine the light in the vertical direction. The three waveguides at the right are defined to test the leakage of the bend in the straight forward and 45 degree directions.

The optical properties of the amorphous silicon guiding layer were measured by variable angle spectroscopic ellipsometry (not shown). The refractive index of a-Si is 3.73 at 1.5 μm , significantly higher than that of crystalline silicon ($n = 3.44$). This result is similar to that found for amorphous silicon made by ion irradiation with different ions.²⁵ Ellipsometry and transmission measurements on 2 μm thick a-Si layers gave no indication for measurable absorption, suggesting that the absorption coefficient is smaller than $\sim 50 \text{ cm}^{-1}$. Hence, a-Si will be a suitable waveguide material in a photonic crystal with dimensions of the order of 10 μm . However, no measurable transmission was observed through the input and output waveguides, which are of order mm length, indicating that the absorption coefficient is larger than $\sim 15 \text{ cm}^{-1}$. Future work will focus on reducing the absorption losses of a-Si.

Figure 7c shows a cross-section made by fluorescence confocal microscopy of Si pillars coated with a SiO_2 layer containing eosin-ITC fluorescent dye. From this image it can be seen that the full surface of the structure is covered with a fluorescent layer. Although the pillars in this image are much wider than those needed for photonic crystals operating around 1.5 μm , these results show that it is possible to coat micrometer size structures with a fluorescent layer by means of a wet chemical process at room temperature. By using other luminescent species that luminesce at wavelengths in the photonic bandgap region, the influence of a 2-D photonic crystal on spontaneous emission can be studied. For instance, similar oxide films on a stratified substrate doped with erbium ions show clear photoluminescence around 1.5 μm with a luminescence lifetime as long as 5.5 ms, and a quantum efficiency of $\sim 38\%$, depending on the Er concentration.

4. Conclusions

The spontaneous emission of Cr ions implanted into Al_2O_3 and Er ions implanted in 100 nm thick SiO_2 layers on Si was influenced by covering the samples with different refractive

index liquids. The measured changes in spontaneous emission rate of the atoms were compared to a calculation of the optical density-of-states. The experimental data can be fitted by assuming both radiative and non-radiative decay processes. From these fits a radiative decay rate of $164 \pm 10 \text{ s}^{-1}$ was determined for Cr ions in Al_2O_3 independent of Cr concentration. For the Er implanted SiO_2 samples a radiative decay rate of $48 \pm 10 \text{ s}^{-1}$ was found, which was then used to study the reduction of spontaneous emission rate in Er doped colloidal spheres with a diameter of 339 nm. The colloids surrounded by air show an Er decay rate as low as $69 \pm 10 \text{ s}^{-1}$. By index matching the spheres, the emission rate was found to be increased by a factor of 2-4.

Bandstructure calculations were performed for a square lattice of Si cylinders and show bandgaps for TM polarization only. For a radius-to-pitch ratio of 0.18 a bandgap was found for $\omega a/2\pi c = 0.30$ to 0.44. Devices for a wavelength of 1.5 μm using this photonic bandgap were fabricated using deep anisotropic etching of 205 nm diameter cylinders on a square lattice with a pitch of 570 nm in a SF_6/O_2 plasma. Vertical confinement may be provided by etching 5 μm long cylinders through a 2 μm thick amorphous Si layer ($n = 3.73$) on crystalline Si. Coating of Si cylinders with SiO_2 layers containing a luminescent dye was achieved using a wet chemical process. Similar layers can be used to probe spontaneous emission in 2-D photonic crystals.

Acknowledgments

We would like to acknowledge Ad Lagendijk and Adriaan Tip for stimulating discussions. This work is part of the research program of the foundation for fundamental research on matter (FOM) and was made possible by financial support of the Dutch organization for scientific research (NWO).

References

- ¹ E.M. Purcell, Spontaneous emission probabilities at radio frequencies, *Phys. Rev.* **69**, 681 (1946).
- ² K.H. Drexhage, Influence of a dielectric interface on fluorescence decay time, *J. Lumin.* **1,2**, 693 (1970).
- ³ R.G. Hulet, E.S. Hilfer, and D. Kleppner, Inhibited spontaneous emission by a Rydberg atom, *Phys. Rev. Lett.* **55**, 2137 (1985).
- ⁴ A.M. Vredenberg, N.E.J. Hunt, E.F. Schubert, D.C. Jacobson, J.M. Poate, and G.J. Zyzik, Controlled spontaneous emission from Er^{3+} in a transparent Si/ SiO_2 microcavity, *Phys. Rev. Lett.* **71**, 517 (1993).
- ⁵ E. Snoeks, A. Lagendijk, and A. Polman, Measuring and modifying the spontaneous emission rate of erbium near an interface, *Phys. Rev. Lett.* **74**, 2459 (1995)
- ⁶ W.L. Barnes, Topical review: Fluorescence near interfaces: the role of photonic mode density, *J. Mod. Opt.* **45**, 661 (1998).
- ⁷ A. van Blaaderen, and A. Vrij, Synthesis and characterization of colloidal dispersions of fluorescent monodisperse silica spheres, *Langmuir* **8**, 2921 (1993).
- ⁸ L.H. Slooff, M.J.A. de Dood, A. van Blaaderen, and A. Polman, Erbium-implanted silica colloids with 80% luminescence quantum efficiency, *Appl. Phys. Lett.* **76**, 3682 (2000).
- ⁹ T.M. Hensen, M.J.A. de Dood, and A. Polman, Luminescence quantum efficiency and local optical density of states in thin film ruby made by ion implantation, (unpublished).
- ¹⁰ H. Khosravi, and R. Loudon, Vacuum field fluctuation and spontaneous emission in the vicinity of a dielectric surface, *Proc. R. Soc. Lond. A* **433**, 337 (1991).
- ¹¹ H.P. Urbach, and G.L.J.A. Rikken, Spontaneous emission from a dielectric slab, *Phys. Rev. A* **57**, 3913 (1998).

- ¹² B.A. van Tiggelen, and E. Kogan, Analogies between light and electrons: Density of states and Friedel's identity, *Phys. Rev. A* **75**, 422 (1995).
- ¹³ F.J.P. Schuurmans, D.T.N. de Lang, G.H. Wegdam, R. Sprik, and A. Lagendijk, Local-field effects on spontaneous emission in a dense supercritical gas, *Phys. Rev. Lett.* **80**, 5077 (1998).
- ¹⁴ R. Sprik, B.A. van Tiggelen, and A. Lagendijk, Optical emission in periodic dielectrics, *Europhys. Lett.* **35**, 265 (1996).
- ¹⁵ J.B. Pendry, and A. MacKinnon, Calculation of photon dispersion relations, *Phys. Rev. Lett.* **69**, 2772 (1992).
- ¹⁶ J.D. Joannopoulos, R.D. Meade, and J.N. Winn, *Photonic Crystals: Molding the Flow of Light*, Princeton University Press (1995).
- ¹⁷ A. Mekis, J.C. Chen, I. Kurland, S. Fan, and J.D. Joannopoulos, High transmission through sharp bends in photonic crystal waveguides, *Phys. Rev. Lett.* **77**, 3787 (1996).
- ¹⁸ S.Y. Lin, E. Chow, and V. Hietala and P.R. Villeneuve and J.D. Joannopoulos, Experimental demonstration of guiding and bending of electromagnetic waves in a photonic crystal, *Science* **282**, 274 (1998).
- ¹⁹ M.J.A. de Dood, E. Snoeks, A. Moroz, and A. Polman, Design and optimization of 2-D photonic crystal waveguides based on silicon, (unpublished).
- ²⁰ S. Roorda, W.C. Sinke, J.M. Poate, D.C. Jacobson, S. Dierker, B.S. Dennis, D.J. Eaglesham, F. Spaepen, and P. Fuoss, Structural relaxation and defect annihilation in pure amorphous silicon, *Phys. Rev. B* **44**, 3702 (1991).
- ²¹ N.A.M. Verhaegh, and A. van Blaaderen, Dispersions of Rhodamine-labeled silica spheres - synthesis, characterization and fluorescence confocal scanning laser microscopy, *Langmuir* **10**, 1427 (1994).
- ²² S. Tachi, K. Tsujimoto, S. Arai and T. Kure, Low-temperature dry etching, *J. Vac. Sci. Technol. A* **9**, 796 (1991).
- ²³ J.K. Bhardwaj, and H. Ashraf, Advanced silicon etching using high density plasmas, *SPIE* **2639**, 224 (1995).
- ²⁴ T. Zijlstra, E. van der Drift, M.J.A. de Dood, E. Snoeks, and A. Polman, Fabrication of two-dimensional photonic crystal waveguides at 1.5 μm in silicon by deep anisotropic etching, *J. Vac. Sci. Technol. B* **17**, 2734 (1999).
- ²⁵ C.N. Waddell, W.G. Spitzer, J.E. Fredrickson, G.K. Hubler, and T.A. Kennedy, Amorphous silicon produced by ion implantation: Effects of ion mass and thermal annealing, *J. Appl. Phys.* **55**, 4361 (1984).